

A mixed-categorical correlation kernel for Gaussian process

P. Saves* Y. Diouane† N. Bartoli‡ T. Lefebvre§ J. Morlier¶

Abstract

Recently, there has been a growing interest for mixed-categorical meta-models based on Gaussian process (GP) surrogates. In this setting, several existing approaches use different strategies either by using continuous kernels (*e.g.*, continuous relaxation and Gower distance based GP) or by using a direct estimation of the correlation matrix. In this paper, we present a kernel-based approach that extends continuous exponential kernels to handle mixed-categorical variables. The proposed kernel leads to a new GP surrogate that generalizes both the continuous relaxation and the Gower distance based GP models. We demonstrate, on both analytical and engineering problems, that our proposed GP model gives a higher likelihood and a smaller residual error than the other kernel-based state-of-the-art models. Our method is available in the open-source software SMT.

1 Introduction

Expensive-to-evaluate blackbox simulations play a key role for many engineering and industrial applications. In this context, surrogate models have shown great interest for a wide range of applications, *e.g.*, aircraft design [1], deep neural networks [2], coastal flooding prediction [3], agriculture forecasting [4] or seismic imaging [5]. These blackbox simulations are generally complex and may involve mixed-categorical input variables. Typically, an aircraft design tool has to take into account variables such as the number of panels, the list of cross sectional areas or the material choices.

In this work, we target to learn an inexpensive surrogate model \hat{f} from a mixed-categorical blackbox function given by

$$f : \Omega \times S \times \mathbb{F}^l \rightarrow \mathbb{R}. \quad (1)$$

This function f is typically an expensive-to-evaluate simulation with no exploitable derivative information. $\Omega \subset \mathbb{R}^n$ represents the bounded continuous design set for the n continuous variables. $S \subset \mathbb{Z}^m$ represents the bounded integer set where L_1, \dots, L_m are the numbers of levels of the m quantitative integer variables on which we can define an order relation and $\mathbb{F}^l = \{1, \dots, L_1\} \times \{1, \dots, L_2\} \times \dots \times \{1, \dots, L_l\}$ is the design space for the l categorical qualitative variables with their respective L_1, \dots, L_l levels.

*ONERA/DTIS & ISAE-SUPAERO, Université de Toulouse, France. E-mail: paul.saves@isae-supaero.fr

†MAGI, Polytechnique Montréal, Canada. E-mail: youssef.diouane@polymtl.ca

‡ONERA/DTIS, Université de Toulouse, France. E-mail: nathalie.bartoli@onera.fr

§ONERA/DTIS, Université de Toulouse, France. E-mail: thierry.lefebvre@onera.fr

¶ICA, Université de Toulouse, ISAE-SUPAERO, MINES ALBI, UPS, INSA, CNRS, Toulouse, France. E-mail: joseph.morlier@isae-supaero.fr

For that purpose, *Gaussian process* (GP) [6], also called Kriging model [7], is known to be a good modeling strategy to learn a response surface model from a given dataset. Namely, we will consider that our unknown blackbox function f follows a Gaussian process of mean μ^f and of standard deviation σ^f , *i.e.*,

$$f \sim \hat{f} = \text{GP} \left(\mu^f, [\sigma^f]^2 \right). \quad (2)$$

For a general problem involving categorical or integer variables, several modeling strategies to build a mixed-categorical GP have been proposed [1, 8–14]. Compared to a continuous GP, the major changes are in the estimation of the correlation matrix, the latter being essential to build estimates of μ^f and σ^f . Similarly to the process of constructing a GP with continuous inputs, relaxation techniques [1, 12], continuous latent variables [14] and Gower distance based models [13] use a kernel-based approach to estimate the correlation matrix. Other recent approaches try to estimate the correlation matrix independently of a kernel choice by modeling directly the possible correlation entries of the correlation matrix [8–11].

Using GP surrogates is not the only possible approach whatsoever. Random forests are often used instead of GP as they also can model both mean and variance [15] and tree-structured Parzen estimators have been shown to be well-adapted for such problems [16]. Other surrogate models for blackbox include ReLU functions [17], piecewise linear neural network [18] or categorical regression splines [19]. Models other than GP could also be based on a mixed integer kernel as for support vector regression [20] or on a mixed integer distance as for radial basis functions [21]. Another classical modeling strategy is to consider a different continuous model for every possible categorical choice and to build another model peculiar to the categorical variables besides the continuous models. This categorical model can be, for instance, a probability law [22], a multi-arm bandit [23] or an integer model [24]. Also, in case of prior information, latent variables approaches [14] and user-defined neighbourhood [25] based models are of great interest, especially for engineering problems.

In this paper, we target to extend the classical paradigm for continuous inputs (where a kernel is used to build the GP) to cover the mixed-categorical case. Namely, we will present a kernel-based approach that will lead to a unified model for existing approximation strategies [8, 12, 13]. This work generalizes existing methods that were already proven to be efficient over deep learning models [12] and analytical test cases [13]. A similar kernel for the estimation of the correlation matrix could be applied to continuous, integer and categorical inputs. The good potential of the proposed approach is shown and analyzed over analytical and industrial test cases.

The GP models and the Bayesian Optimization (BO) that could be performed with them are implemented in the Surrogate Modeling Toolbox (SMT) v1.4¹. The latter modeling toolbox is developed by ONERA, ISAE-Supaero, ICA (CNRS), NASA Glenn and the University of Michigan [26]. Our modeling software is free and open-source and has been used regularly in the aircraft industry, for example with a deep learning model [27–30] or with a deep gaussian process [31, 32].

The reminder of this paper is as follows. In Section 2, a detailed review of the GP model for continuous and for categorical inputs is given. The extended kernel-based approach for constructing the correlation matrix is presented in Section 3. Section 4 presents academical tests as well as the obtained results. Conclusions and perspectives are finally drawn in Section 5.

¹<https://smt.readthedocs.io/en/latest/>

2 GP for mixed-categorical inputs

In this section, we will present the mathematical background associated with GP for mixed-categorical variables. This part also introduces the notations that will be used throughout the paper. In this section, we are considering the general case involving mixed integer variables. Namely, we assume that $f : \mathbb{R}^n \times \mathbb{Z}^m \times \mathbb{F}^l \mapsto \mathbb{R}$ and our goal is to build a GP surrogate model for f .

Given a set of data points, called a Design of Experiments (DoE) [33], Bayesian inference learns the GP model that explains the best this data set. A GP model consists of a mean response hypersurface μ^f , as well as an estimation of its variance $[\sigma^f]^2$. In the following, n_t denotes the size of the given DoE data set (W, \mathbf{y}^f) such that $W = \{w^1, w^2, \dots, w^{n_t}\} \in (\mathbb{R}^n \times \mathbb{Z}^m \times \mathbb{F}^l)^{n_t}$ and $\mathbf{y}^f = [f(w^1), f(w^2), \dots, f(w^{n_t})]^\top$. For an arbitrary $w = (x, z, c) \in \mathbb{R}^n \times \mathbb{Z}^m \times \mathbb{F}^l$, not necessary in the DoE, the GP model prediction at w writes as $\hat{f}(w) = \mu(w) + \epsilon(w) \in \mathbb{R}$, with ϵ being the error between f and the model approximation μ [34]. The considered error terms are random variables of variance σ^2 . Using the DoE, the expression of μ^f and the estimation of its variance $[\sigma^f]^2$ are given as follows:

$$\mu^f(w) = \hat{\mu}^f + r(w)^\top [R(\Theta)]^{-1} (\mathbf{y}^f - \mathbf{1} \hat{\mu}^f), \quad (3)$$

and

$$[\sigma^f(w)]^2 = [\hat{\sigma}^f]^2 \left[1 - r(w)^\top [R(\Theta)]^{-1} r(w) + \frac{(1 - \mathbf{1}^\top [R(\Theta)]^{-1} r(w))^2}{\mathbf{1}^\top [R(\Theta)]^{-1} \mathbf{1}} \right], \quad (4)$$

where $\hat{\mu}^f$ and $\hat{\sigma}^f$, respectively, are the maximum likelihood estimator (MLE) [35] of μ and σ . $\mathbf{1}$ denotes the vector of n_t ones. R is the $n_t \times n_t$ correlation matrix between the input points and $r(w)$ is the correlation vector between the input points and a given w . The correlation matrix R is defined, for a given couple $(r, s) \in (\{1, \dots, n_t\})^2$, by

$$[R(\Theta)]_{r,s} = k(w^r, w^s, \Theta) \in \mathbb{R}, \quad (5)$$

and the vector $r(w) \in \mathbb{R}^{n_t}$ is defined as $r(w) = [k(w, w^1), \dots, k(w, w^{n_t})]^\top$, where k is a given correlation kernel that relies on a set of hyperparameters Θ [11]. The mixed-categorical correlation kernel is given as the product of three kernels:

$$k(w^r, w^s, \Theta) = k^{cont}(x^r, x^s, \theta^{cont}) k^{int}(z^r, z^s, \theta^{int}) k^{cat}(c^r, c^s, \theta^{cat}), \quad (6)$$

where k^{cont} and θ^{cont} are the continuous kernel and its associated hyperparameters, k^{int} and θ^{int} are the integer kernel and its hyperparameters, and last k^{cat} and θ^{cat} are the ones related with the categorical inputs. In this case, one has $\Theta = \{\theta^{cont}, \theta^{int}, \theta^{cat}\}$. Henceforth, the general correlation matrix R will rely only on the set of the hyperparameters Θ :

$$[R(\Theta)]_{r,s} = [R^{cont}(\theta^{cont})]_{r,s} [R^{int}(\theta^{int})]_{r,s} [R^{cat}(\theta^{cat})]_{r,s}, \quad (7)$$

where $[R^{cont}(\theta^{cont})]_{r,s} = k^{cont}(x^r, x^s, \theta^{cont})$, $[R^{int}(\theta^{int})]_{r,s} = k^{int}(z^r, z^s, \theta^{int})$ and $[R^{cat}(\theta^{cat})]_{r,s} = k^{cat}(c^r, c^s, \theta^{cat})$. The set of hyperparameters Θ could be estimated using the DoE data set (W, \mathbf{y}^f) through the MLE approach on the following way

$$\Theta^* = \arg \max_{\Theta} \mathcal{L}(\Theta) := \left(-\frac{1}{2} \mathbf{y}^{f\top} [R(\Theta)]^{-1} \mathbf{y}^f - \frac{1}{2} \log |[R(\Theta)]| - \frac{n_t}{2} \log 2\pi \right), \quad (8)$$

where $R(\Theta)$ is computed using Eq. (7). To construct the correlation matrix, several choices for the correlation kernel are possible. Usual families of kernels include exponential kernels or Matern kernels [36]. In the rest of this section, we will focus mainly on the exponential kernels and describe in details the construction of the continuous $R^{cont}(\theta^{cont})$, the integer $R^{int}(\theta^{int})$ and the categorical $R^{cat}(\theta^{cat})$ correlation matrices.

2.1 Correlation matrices for continuous and integer inputs

The construction of the correlation matrix $R^{cont}(\theta^{cont})$ for continuous inputs, based on an exponential kernel, can be described as follows. For a couple of continuous inputs $x^r \in \mathbb{R}^n$ and $x^s \in \mathbb{R}^n$, one sets

$$[R^{cont}(\theta^{cont})]_{r,s} = \prod_{j=1}^n \exp(-\theta_j^{cont} |x_j^r - x_j^s|^p). \quad (9)$$

Different values for p can be used. Typically, when $p = 1$, one gets the absolute exponential kernel (Ornstein-Uhlenbeck process [36]) and, when $p = 2$, the squared exponential kernel (or Gaussian kernel [6]) is obtained. Clearly, in the continuous case, constructing $R^{cont}(\theta^{cont})$ would require the estimation of n non-negative hyperparameters, *i.e.*, $\theta^{cont} \in \mathbb{R}_+^n$.

Thanks to a continuous relaxation technique that transforms integer inputs into continuous ones, the integer inputs can be naturally handled with continuous kernels. On this base, in what comes next, there will be no distinction between continuous and integer inputs; the two of them will be handled in the same way. In fact, for integer variables, the distance defined in the continuous case is still valid. Thus, for an integer couple $z^r \in \mathbb{Z}^m$ and $z^s \in \mathbb{Z}^m$, a natural extension of the exponential kernel that handles integer variables can be given as follows:

$$[R^{int}(\theta^{int})]_{r,s} = \prod_{j=1}^m \exp(-\theta_j^{int} |z_j^r - z_j^s|^p). \quad (10)$$

In a similar fashion, constructing $R^{int}(\theta^{int})$ would require the estimation of m non-negative hyperparameters, *i.e.*, $\theta^{int} \in \mathbb{R}_+^m$.

2.2 Correlation matrices for categorical inputs

For categorical inputs, different choices can be made to build the correlation matrix $R^{cat}(\theta^{cat})$. Some choices are sophisticated and can therefore lead to better GP models, but are known to be computationally expensive (particularly as the number of categorical inputs increases) [8, 11]. On the contrary, simple extensions of the well-known continuous kernels based on the Gower distance [13] or on the continuous relaxation techniques [37] would be less expensive. In the rest of this section, we will describe three known techniques to build correlation matrices for categorical inputs that are based on kernels.

2.2.1 Gower distance based kernel

The Gower distance based kernel dedicates one hyperparameter per categorical input variable [13, 38]. This method uses the notion of Hamming distance between categorical inputs to naturally extend continuous correlation kernel functions. Namely, for two given inputs $c^r \in \mathbb{F}^l$ and $c^s \in \mathbb{F}^l$,

the Hamming distance, or score, s between the i^{th} component of c^r and c^s is defined as: $s(c_i^r, c_i^s) = 1$ if $c_i^r = c_i^s$, otherwise $s(c_i^r, c_i^s) = 0$. Thanks to the Hamming distance, one can straightforwardly use a continuous kernel to define $R^{cat}(\theta^{cat})$. For instance, in the case of an exponential kernel, the Gower distance based correlation matrix will be given by

$$[R^{cat}(\theta^{cat})]_{r,s} = k^{cat}(c^r, c^s, \theta^{cat}) = \prod_{i=1}^l \exp(-\theta_i^{cat} s(c_i^r, c_i^s)^p).$$

Similarly to the continuous and integer correlation matrices, the construction of the categorical correlation matrix based on the Gower distance kernel requires the estimation of l hyperparameters ($\theta^{cat} \in \mathbb{R}_+^l$). Note that, as the Hamming distance can only take the values 0 and 1, all the exponential kernels lead to the same result independently of the value of p .

2.2.2 Continuous relaxation based kernel

To handle categorical variables through continuous relaxation, the design space \mathbb{F}^l is relaxed to a continuous space Ω^l constructed in the following way. For a given $i \in \{1, \dots, l\}$, let c_i be the i^{th} categorical variable with L_i levels, and, for a given input point c^r , let ℓ_r^i be the index of the level taken by c^r on the variable i . Denote $e_{c_i^r}$ the one-hot encoding [37] of c_i^r that takes value 1 everywhere but on the dimension ℓ_r^i : $e_{c_i^r} \in \mathbb{R}^{L_i}$ such that $(e_{c_i^r})_{\ell_r^i} = 1$ and $(e_{c_i^r})_k = 0$ for $k \neq \ell_r^i$. For example, if the i^{th} component is the color with $L_i = 3$ levels being {red, blue, green} and if the r^{th} variable takes value blue ($c_i^r = \text{blue}$), then the corresponding index is $\ell_r^i = 2$ and the corresponding one-hot encoding is $e_{c_i^r} = (0, 1, 0)$. The continuous relaxation idea is as follows. At the beginning we set Ω^l to be empty, then, for each $i \in \{1, \dots, l\}$, a relaxed one-hot encoding is used for c_i . The latter increases the dimension of the relaxed continuous space Ω^l by L_i and, at the end of the relaxation, we get the final continuous design space $\Omega^l \subseteq \{0, 1\}^{n^l}$, where $n^l = \sum_{i=1}^l L_i > l$.

Like the Gower distance based kernel, the continuous relaxation based kernel adapts continuous kernels to handle categorical variables, *i.e.*, for a couple of categorical inputs c^r and c^s ,

$$[R^{cat}(\theta^{cat})]_{r,s} = k^{cat}(c^r, c^s, \theta^{cat}) = \prod_{i=1}^l k^{cat}(c_i^r, c_i^s, \theta^{cat}) = \prod_{i=1}^l \prod_{j=1}^{L_i} k^{cont}([e_{c_i^r}]_j, [e_{c_i^s}]_j, \theta^{cat}).$$

Typically, for an exponential continuous kernel, one has

$$[R^{cat}(\theta^{cat})]_{r,s} = \prod_{i=1}^l \prod_{j=1}^{L_i} \exp\left(-\theta_{\sum_{i'=1}^{i-1} L_{i'} + j}^{cat} |[e_{c_i^r}]_j - [e_{c_i^s}]_j|^p\right), \quad (11)$$

and, by using the one-hot encoding structure of $e_{c_i^r}$ and $e_{c_i^s}$, it leads to

$$[R^{cat}(\theta^{cat})]_{r,s} = \prod_{i=1}^l \exp\left(-\theta_{\sum_{i'=1}^{i-1} L_{i'} + \ell_r^i}^{cat} - \theta_{\sum_{i'=1}^{i-1} L_{i'} + \ell_s^i}^{cat}\right).$$

Hence, this kernel relies on $n^l = \sum_{i=1}^l L_i$ hyperparameters ($\theta^{cat} \in \mathbb{R}_+^{n^l}$) which can be much more higher than the number of hyperparameters required to build the Gower distance based kernel. Due to one-hot encoding strategy, the value of p is also irrelevant for the construction of the continuous relaxation based kernel.

2.2.3 Homoscedastic hypersphere kernel

The idea of the homoscedastic hypersphere kernel [8, 11] is to directly model the correlation matrix instead of looking for a kernel function. The use of a kernel function guarantees the related correlation matrix R^{cat} to be symmetric positive definite (SPD). However, with the homoscedastic hypersphere kernel, one will directly construct an SPD matrix with the desired properties. Namely, for a given $i \in \{1, \dots, l\}$, let c_i^r and c_i^s be a couple of categorical variables taking respectively the ℓ_r^i and the ℓ_s^i level on the categorical variable c_i , $[R^{cat}(\theta^{cat})]_{r,s}$ can be formulated in a level-wise form [8] as:

$$[R^{cat}(\theta^{cat})]_{r,s} = k^{cat}(c^r, c^s, \theta^{cat}) = \prod_{i=1}^l [R_i(\Theta_i)]_{\ell_r^i, \ell_s^i} = \prod_{i=1}^l [C(\Theta_i)C(\Theta_i)^\top]_{\ell_r^i, \ell_s^i}. \quad (12)$$

For all $i \in \{1, \dots, l\}$, the matrix $C(\Theta_i) \in \mathbb{R}^{L_i \times L_i}$ is lower triangular and built using a hypersphere decomposition [39, 40] from a symmetric matrix $\Theta_i \in \mathbb{R}^{L_i \times L_i}$ of hyperparameters. For any $k, k' \in \{1, \dots, L_i\}$, the matrix $C(\Theta_i)$ is given by:

$$\begin{cases} [C(\Theta_i)]_{1,1} = 1 \\ [C(\Theta_i)]_{k,1} = \cos([\Theta_i]_{k,1}) \text{ for any } 2 \leq k \leq L_i \\ [C(\Theta_i)]_{k,k'} = \cos([\Theta_i]_{k,k'}) \prod_{j=1}^{k'-1} \sin([\Theta_i]_{k,j}), \text{ for any } 2 \leq k' < k \leq L_i \\ [C(\Theta_i)]_{k,k} = \prod_{j=1}^{k-1} \sin([\Theta_i]_{k,j}), \text{ for any } 2 \leq k \leq L_i, \end{cases} \quad (13)$$

where the hyperparameters are set such that $[\Theta_i]_{k,k'} \in [0, \pi]$ for all $1 \leq k' < k \leq L_i$. For this kernel, the hyperparameters θ^{cat} can be seen as a concatenation of the set of symmetric matrices, *i.e.*, $\theta^{cat} = \{\Theta_1, \Theta_2, \dots, \Theta_l\}$. The construction of this kernel is thus relying on the estimation of $\sum_{i=1}^l \frac{1}{2} L_i(L_i - 1)$ hyperparameters. Unlike the previous kernels where the elements of the correlation matrix are non-negative, the correlation values for the homoscedastic hypersphere kernel can be negative, *i.e.*, $[R^{cat}(\theta^{cat})]_{r,s} \in [-1, 1]$.

3 An exponential kernel-based model for categorical inputs

In this section, we propose an extension of the classical exponential kernels (used for continuous inputs) to handle categorical variables. Thanks to the one-hot encoding, we can replace the distance-based approach by an hyperparameter-based approach. This extension will naturally lead to a generalization of both continuous relaxation and Gower distance based kernels.

Distance based approaches (like Gower distance or continuous relaxation) can not model every possible correlation between the various categorical choices. Therefore, these methods do not lead to an exhaustive GP model but to an imprecise approximation. In what follows, we propose to introduce a new formulation that includes a correlation matrix so that we could reach a higher accuracy for the resulting distance-based GP model. To begin with, the continuous relaxation kernel described in Eq. (11) can be reformulated as:

$$[R^{cat}(\theta^{cat})]_{r,s} = \prod_{i=1}^l \prod_{j=1}^{L_i} \exp\left(-|e_{c_i^r} - e_{c_i^s}|_j^{p/2} [\Theta_i]_{j,j} |e_{c_i^r} - e_{c_i^s}|_j^{p/2}\right), \quad (14)$$

where, for all $i = 1, \dots, l$, the matrix $\Theta_i \in \mathbb{R}^{L_i \times L_i}$ is diagonal such that $[\Theta_i]_{j,j} = \theta_{\sum_{i'=1}^{i-1} L_{i'} + j}^{cat} \in \mathbb{R}_+$, and θ^{cat} is defined as the list of hyperparameter matrices $\theta^{cat} = \{\Theta_1, \dots, \Theta_l\}$. The idea of the new kernel is the following: we start from the reformulation of the continuous relaxation kernel of Eq. (14). Then, as for the kernel of Eq. (12), we consider, for every categorical variable $i = 1, \dots, l$, a SPD matrix $\Phi(\Theta_i) \in \mathbb{R}^{L_i \times L_i}$ used to build a kernel associated with the correlation matrix $R_i(\Phi(\Theta_i))$. Let c_i^r and c_i^s be a couple of categorical variables taking respectively the ℓ_r^i and the ℓ_s^i level of the variable c_i , we set

$$[R^{cat}(\theta^{cat})]_{r,s} = \prod_{i=1}^l [R_i(\Phi(\Theta_i))]_{\ell_r^i, \ell_s^i}, \quad (15)$$

and, for all $i = 1, \dots, l$, one has

$$[R_i(\Phi(\Theta_i))]_{\ell_r^i, \ell_s^i} = \prod_{j=1}^{L_i} \prod_{j'=1}^{L_i} \exp \left(- |e_{c_i^r} - e_{c_i^s}|_j^{p/2} [\Phi(\Theta_i)]_{j,j'} |e_{c_i^r} - e_{c_i^s}|_{j'}^{p/2} \right), \quad (16)$$

where ℓ_r^i and ℓ_s^i are the indices of the levels taken by the variables c^r and c^s , respectively, on the i^{th} categorical variable and the coefficient $[\Phi(\Theta_i)]_{\ell_r^i, \ell_s^i}$ is characterizing the correlation between this two levels.

Remark 1. One can easily see that Eq. (16) generalizes the continuous relaxation approach. In fact, by setting $\Phi(\Theta_i) = \Theta_i$ to be a diagonal matrix, we recover Eq. (14).

Now, by using the one-hot encoding nature of the vectors $e_{c_i^r}$ and $e_{c_i^s}$, we get naturally what follows. Namely, if $c_i^r = c_i^s$, one deduces that $[R_i(\Phi(\Theta_i))]_{\ell_r^i, \ell_s^i} = \exp(0) = 1$. Otherwise, if $c_i^r \neq c_i^s$, we get

$$\begin{aligned} [R_i(\Phi(\Theta_i))]_{\ell_r^i, \ell_s^i} &= \exp \left(- \sum_{j=1}^{L_i} \sum_{j'=1}^{L_i} |e_{c_i^r} - e_{c_i^s}|_j^{p/2} [\Phi(\Theta_i)]_{j,j'} |e_{c_i^r} - e_{c_i^s}|_{j'}^{p/2} \right) \\ &= \exp \left(- ([\Phi(\Theta_i)]_{\ell_r^i, \ell_r^i} + [\Phi(\Theta_i)]_{\ell_s^i, \ell_s^i} + [\Phi(\Theta_i)]_{\ell_r^i, \ell_s^i} + [\Phi(\Theta_i)]_{\ell_s^i, \ell_r^i}) \right) \\ &= \exp \left(- [\Phi(\Theta_i)]_{\ell_r^i, \ell_r^i} - [\Phi(\Theta_i)]_{\ell_s^i, \ell_s^i} - 2[\Phi(\Theta_i)]_{\ell_r^i, \ell_s^i} \right). \end{aligned} \quad (17)$$

Remark 2. Note that the resulting correlation matrix $R_i(\Phi(\Theta_i))$ does not depend on the chosen parameter p (used within the definition of the exponential kernels). Therefore, in our case, when dealing with categorical variables kernels, there will be no distinction between squared or absolute exponential kernels.

In addition, as far as the matrices Θ_i respect a specific parameterization, we will show that our approach guarantees that the correlation matrix R is SPD with a unit diagonal and off-diagonal terms value in $[0, 1]$ [41]. In general, the latter properties are required to be satisfied by the correlation matrices. Otherwise, one may get numerical issues to build the GP model, see Eq. (3) and Eq. (4). For that purpose, for a given $i \in \{1, \dots, l\}$, we propose to use the following parameterization for the hyperparameter matrix $\Phi(\Theta_i)$:

$$\begin{aligned} [\Phi(\Theta_i)]_{j,j} &:= [\Theta_i]_{j,j} \geq 0 \\ [\Phi(\Theta_i)]_{j,j'} &:= \frac{\log \epsilon}{2} ([C(\Theta_i)C(\Theta_i)^\top]_{j,j'} - 1) \quad \text{if } j \neq j', \end{aligned} \quad (18)$$

where the parameter ϵ is chosen as a small positive tolerance ($0 < \epsilon \ll 1$) and the matrix $C(\Theta_i)$ is a Cholesky lower triangular matrix that relies on the symmetric matrix Θ_i of $L_i(L_i-1)/2$ elements in $[0, \frac{\pi}{2}]$. The elements of $C(\Theta_i)$ represents the coordinates of a point on the surface of a unit radius sphere as in [8, 11]. They are described in Eq. (13). Note that, by taking into consideration the symmetry of the matrix Θ_i , the total number of hyperparameters for the categorical variable i is $\frac{L_i(L_i+1)}{2}$.

In the next theorem, we will show that the parameterization given by Eq. (18) guarantees the desirable properties for the correlation matrices $R_i(\Theta_i)$ and therefore for the matrix R^{cat} . In particular, we will show that the matrix $R^{cat}(\theta^{cat})$ is SPD with elements in $[0, 1]$, *i.e.*, for all $s, r \in \{1, \dots, n_t\}$, $[R^{cat}(\theta^{cat})]_{r,s} \in [0, 1]$.

Theorem 1. *Assume that, for all $i \in \{1, \dots, l\}$, $\Phi(\Theta_i)$ satisfies the parameterization of Eq. (18). Then the matrix $R^{cat}(\theta^{cat})$, given by Eq. (15), is SPD with elements in $[0, 1]$.*

Proof. Indeed, for all $i \in \{1, \dots, l\}$, by using Eq. (17) and Eq. (18), one has

$$\begin{aligned} [R_i(\Phi(\Theta_i))]_{\ell_r^i, \ell_s^i} &= [W_i]_{\ell_r^i, \ell_s^i} [T_i]_{\ell_r^i, \ell_s^i}, \quad \text{if } \ell_r^i \neq \ell_s^i \\ [R_i(\Phi(\Theta_i))]_{\ell_r^i, \ell_r^i} &= 1, \end{aligned}$$

where $[W_i]_{\ell_r^i, \ell_s^i} = \exp(-[\Theta_i]_{\ell_r^i, \ell_r^i} - [\Theta_i]_{\ell_s^i, \ell_s^i})$ and $[T_i]_{\ell_r^i, \ell_s^i} = \exp(-2[\Phi(\Theta_i)]_{\ell_r^i, \ell_s^i})$. The matrix $R_i(\Phi(\Theta_i))$ is thus defined as a Hadamard product (*i.e.*, element-wise product of matrices) [42]. Hence, by application of the Schur product theorem [43, Lemma 3.7.1], it suffices to show that the matrices W_i and T_i are SPD to prove that R_i is also SPD. Taking into account that, for all $s, r \in \{1, \dots, n_t\}$, $e_{c_i^r}$ and $e_{c_i^s}$ are one-hot encoding elements of \mathbb{R}^{L_i} , the matrix W_i corresponds to the correlation matrix associated with the exponential kernel in the continuous space, *i.e.*,

$$[W_i]_{\ell_r^i, \ell_s^i} = \exp(-[\Theta_i]_{\ell_r^i, \ell_r^i} - [\Theta_i]_{\ell_s^i, \ell_s^i}) = \prod_{j=1}^{L_i} \exp(-[\Theta_i]_{j,j} |e_{c_i^r} - e_{c_i^s}|_j|^p).$$

Hence, since the diagonal elements of Θ_i are positive, the matrix W_i is SPD. In fact, the kernel function $\phi(x) = \exp[-\theta|x|^p]$ is positive definite for a given positive θ if $0 < p \leq 2$ [44, Corollary 3]. Regarding the matrix T_i , by using the fact that Θ_i satisfies Eq. (18), one has

$$[T_i]_{\ell_r^i, \ell_s^i} = \epsilon \exp\left(-(\log \epsilon)[C(\Theta_i)C(\Theta_i)^\top]_{\ell_r^i, \ell_s^i}\right). \quad (19)$$

For an $\epsilon \in (0, 1)$, the matrix $-(\log \epsilon)[C(\Theta_i)C(\Theta_i)^\top]$ is SPD as a Cholesky like-decomposition matrix. Thus, T_i is also SPD as the Hadamard exponential of an SPD matrix [45, Theorem 7.5.9].

For the second part of the proof, the matrix $C(\Theta_i)$ is constructed by hypersphere decomposition such that the values of $C(\Theta_i)C(\Theta_i)^\top$ belong to $[0, 1]$ [46]. Hence,

$$\begin{aligned} [T_i]_{\ell_r^i, \ell_s^i} &= \epsilon \exp\left(-(\log \epsilon)[C(\Theta_i)C(\Theta_i)^\top]_{\ell_r^i, \ell_s^i}\right) \geq \epsilon \exp 0 = \epsilon, \\ [T_i]_{\ell_r^i, \ell_r^i} &= \epsilon \exp\left(-(\log \epsilon)[C(\Theta_i)C(\Theta_i)^\top]_{\ell_r^i, \ell_r^i}\right) \leq \frac{\epsilon}{\epsilon} = 1. \end{aligned}$$

Also, the elements of the matrix W_i are in $[0, 1]$ since the diagonal elements of Θ_i are chosen to be positive. Consequently, the extra-diagonal elements of R_i are in $[0, 1]$. Finally, the Hadamard product being conservative for those two latter properties, one concludes that the correlation matrix $R^{cat}(\theta^{cat})$ is SPD and all its elements are in $[0, 1]$. \square

Remark 3. For a given small $\epsilon > 0$, the transformation

$$\alpha \rightarrow \epsilon \exp[-\log(\epsilon)(\alpha - 1)] \quad (20)$$

is a bijection over $[\epsilon, 1]$, thus one can deduce that (when $[T_i]_{j,j'} > \epsilon$ for all j, j') there exists a unique matrix $\hat{\Theta}_i$ such that

$$T_i = C(\hat{\Theta}_i)C(\hat{\Theta}_i)^\top.$$

This, in particular, shows that if we set W_i to identity in our parameterization, then, as far as the correlations are larger than ϵ , the homoscedastic hypersphere parameterization of Pelamatti et al. [8, 11] is equivalent to our proposed one.

In the next theorem, using the hypersphere decomposition properties [40], we will show that the correlation matrix R_i , as given by (17), can be built in an equivalent way without the diagonal elements of the matrix $\Phi(\Theta_i)$. Such result is of high interest as it reduces the number of hyperparameters from $\frac{L_i(L_i+1)}{2}$ to $\frac{L_i(L_i-1)}{2}$ per categorical variable i without any loss in the accuracy in the final model.

Theorem 2. The correlation matrix R_i , as given by (17), can be rewritten as follows

$$\begin{aligned} [R_i(\Phi(\bar{\Theta}_i))]_{\ell_r^i, \ell_s^i} &= \exp(-2[\Phi(\bar{\Theta}_i)]_{\ell_r^i, \ell_s^i}), \quad \text{if } \ell_r^i \neq \ell_s^i \\ [R_i(\Phi(\bar{\Theta}_i))]_{\ell_r^i, \ell_r^i} &= 1, \end{aligned} \quad (21)$$

where $[\Phi(\bar{\Theta}_i)]_{\ell_r^i, \ell_s^i} = \frac{\log \epsilon}{2}([C(\bar{\Theta}_i)C(\bar{\Theta}_i)^\top]_{\ell_r^i, \ell_s^i} - 1)$ and $\bar{\Theta}_i$ is a symmetric matrix whose diagonal elements are set to zero (i.e., $[\bar{\Theta}_i]_{j,j} = 0$ for all $j = 1, \dots, L_i$).

Proof. Indeed, by using the hypersphere decomposition [40], any SPD matrix $T_i(\Theta_i)$ with unitary diagonal and values in $[\epsilon, 1]$ can be modeled as $T_i(\Theta_i) = [C(\hat{\Theta}_i)C(\hat{\Theta}_i)^\top]$ from a certain symmetric matrix $\hat{\Theta}_i$ without using additional diagonal elements (i.e., $[\hat{\Theta}_i]_{j,j} = 0$ for all $j = 1, \dots, L_i$). Thus, using the fact that $R_i(\Theta_i)$ is written as the image of this SPD matrix $T_i(\Theta_i)$ by the element-wise transformation of Eq. (20) bijective over $[\epsilon, 1]$, one can deduce that there must exist a symmetric matrix $\bar{\Theta}_i$ whose diagonal elements are set to zero (i.e., $[\bar{\Theta}_i]_{j,j} = 0$ for all $j = 1, \dots, L_i$) such that

$$\begin{aligned} [R_i(\Phi(\bar{\Theta}_i))]_{\ell_r^i, \ell_s^i} &= \exp(-2[\Phi(\bar{\Theta}_i)]_{\ell_r^i, \ell_s^i}), \quad \text{if } \ell_r^i \neq \ell_s^i \\ [R_i(\Phi(\bar{\Theta}_i))]_{\ell_r^i, \ell_r^i} &= 1, \end{aligned}$$

where $[\Phi(\bar{\Theta}_i)]_{\ell_r^i, \ell_s^i} = \frac{\log \epsilon}{2}([C(\bar{\Theta}_i)C(\bar{\Theta}_i)^\top]_{\ell_r^i, \ell_s^i} - 1)$. \square

In what comes next, we will refer to our kernel when it uses the parameterization of Eq. (21) as the Exponential Homoscedastic Hypersphere (EHH) kernel (see Remark 3). We will call the original parameterization of the correlation matrix (as given by (17)) as the Fully Exponential (FE) kernel. Note that, as explained in Appendix 6.1, whenever the matrix Θ_i is chosen to be diagonal, the matrix $\Phi(\Theta_i)$ used within FE kernel will also be diagonal. Thus, we are able to recover the continuous relaxation kernel [12] and this parameterization will be called the Continuous Relaxation (CR) kernel. Similarly, if we choose Θ_i to be of the form $\theta_i \times I_{L_i}$ where $\theta_i \in \mathbb{R}^+$ and I_{L_i} is the identity matrix of size L_i , we are able to recover the Gower distance based kernel [13]: this parameterization will be called the Gower Distance (GD) kernel.

As mentioned earlier, the EHH kernel is similar to the FE kernel. Therefore, we can deduce that the EHH kernel generalizes the CR kernel and also that the CR kernel generalizes the GD

kernel. Table 1 gives all the details associated with the four categorical kernels described above, *i.e.*, GD, CR, EHH and FE.

Table 1: Description of the four categorical kernels (GD, CR, EHH and FE) using our proposed exponential parameterization.

Kernel	$\Theta_i =$	$[R_i(\Theta_i)]_{\ell_r^i, \ell_s^i} =$	# of Hyperparam.
GD	$\theta_i \times \begin{bmatrix} 1 & & & & \textit{Sym.} \\ 0 & 1 & & & \\ \vdots & \ddots & \ddots & & \\ 0 & \dots & 0 & 1 \end{bmatrix}$	$\exp(-2[\Phi(\Theta_i)]_{\ell_r^i, \ell_s^i})$	1
CR	$\begin{bmatrix} [\Theta_i]_{1,1} & & & & \textit{Sym.} \\ 0 & [\Theta_i]_{2,2} & & & \\ \vdots & \ddots & \ddots & & \\ 0 & \dots & 0 & [\Theta_i]_{L_i, L_i} \end{bmatrix}$	$\exp(-[\Phi(\Theta_i)]_{\ell_r^i, \ell_r^i} - [\Phi(\Theta_i)]_{\ell_s^i, \ell_s^i})$	L_i
EHH	$\begin{bmatrix} 0 & & & & \textit{Sym.} \\ [\Theta_i]_{1,2} & 0 & & & \\ \vdots & \ddots & \ddots & & \\ [\Theta_i]_{1, L_i} & \dots & [\Theta_i]_{L_i-1, L_i} & 0 \end{bmatrix}$	$\exp(-2[\Phi(\Theta_i)]_{\ell_r^i, \ell_s^i})$	$\frac{1}{2}L_i(L_i - 1)$
FE	$\begin{bmatrix} [\Theta_i]_{1,1} & & & & \textit{Sym.} \\ [\Theta_i]_{1,2} & [\Theta_i]_{2,2} & & & \\ \vdots & \ddots & \ddots & & \\ [\Theta_i]_{1, L_i} & \dots & [\Theta_i]_{L_i-1, L_i} & [\Theta_i]_{L_i, L_i} \end{bmatrix}$	$\exp(-[\Phi(\Theta_i)]_{\ell_r^i, \ell_r^i} - [\Phi(\Theta_i)]_{\ell_s^i, \ell_s^i} - 2[\Phi(\Theta_i)]_{\ell_r^i, \ell_s^i})$	$\frac{1}{2}L_i(L_i + 1)$

In the next section, we will see how these kernels perform on different test cases. In particular, we will study numerically the trade-off between the kernel efficiencies and their respective computational efforts (related directly to the number of hyperparamters).

4 Results and discussion

In this section, we propose several illustrations and comparisons on four different test cases (from 1 to 10 continuous variables and 1 or 2 categorical variables up to 12 levels) to show the interest of our method and the equivalence with other kernels from the literature. The likelihood value and the approximate errors are the quantities of interest considered to compare different correlation kernels.

4.1 Implementation details

The optimization of the likelihood as a function of the hyperparameters needs a performing gradient-free algorithm, in this work, we are using COBYLA [47] to maximize this quantity from the Python library Scipy with default termination criterion related to the trust region size. As COBYLA is a local search algorithm, a multi-start technique is used. Our models and their

implementation are available in the toolbox SMT v1.2² [26]. By default, in SMT, the number of starting points for COBYLA is equal to 10 with evenly spaced starting points.

A simple noiseless Kriging with a constant prior model for the GP is used. We recall that the absolute exponential kernel and the squared exponential kernel are similar for categorical variables and differ only for the continuous ones. The correlation values range between $2.06\text{e-}9$ and 0.999999 for both continuous and categorical hyperparameters. Therefore, the constant ϵ is chosen to correspond to a correlation value of $2.06\text{e-}9$. The random DoEs are drawn by Latin Hypercube Sampling (LHS) [48] and the validation sets are given by some evenly spaced points.

4.2 Analytic validation

To begin with, the proposed kernels of the previous sections are validated and illustrated over two analytic test cases. The first test case consists of 7 points over a 2D space with one categorical variable and shows how the various categorical kernels can be seen in terms of hyperparameters. The second test case is more complicated and shows the limitations of the kernels in terms of resulting approximated errors.

4.2.1 A 2D problem ($n = 1$, $m = 0$, $l = 1$ and $L_1 = 2$)

We start with a 2D test case with one continuous variable in $[0, 4]$ and one categorical variable with two levels (blue and red). Appendix 6.2 provides a detailed description of the test case. We consider a DoE of 3 blue points and 4 red points. The mixed integer GP model obtained from continuous relaxation is shown in Fig. 1 for its two associated levels (blue and red). Knowing that all methods lead visually to the same GP model (illustrated in Fig. 1), we report only the optimal hyperparameters values in Tab. 2 to illustrate the kernels equivalence.

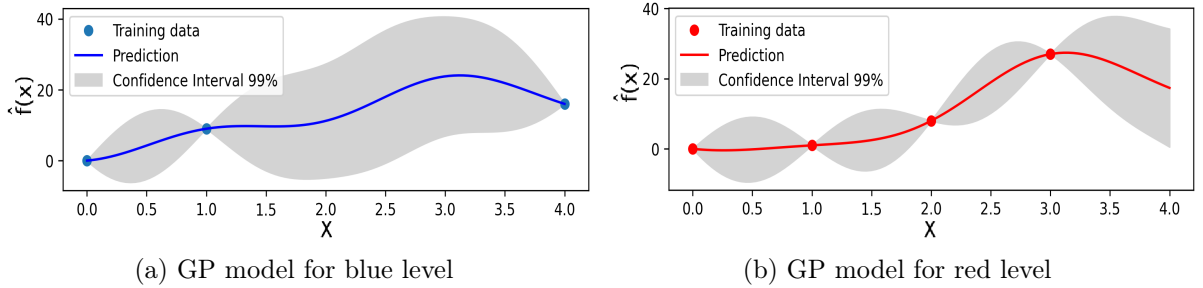


Figure 1: 2D test case Gaussian process for blue and red levels.

²<https://smt.readthedocs.io/en/latest/>

Table 2: Hyperparameter estimations of our proposed model versus existing kernels for the 2D test case.

Tested methods	$\theta_{red,blue}$	$\theta_{red,red}$	$\theta_{blue,blue}$	θ^{cont}
Continuous relaxation [12]	-	0.2300	1.2168e-06	16.576
Our model (with CR kernel)	-	0.2301	8.0294e-06	16.575
Gower distance [13]	0.2300	-	-	16.573
Our model (with GD kernel)	0.2301	-	-	16.573
Homoscedastic hypersphere [8]	0.7944	-	-	16.573
Our model (with EHH kernel)	0.7944	-	-	16.573

In this case, with only two levels, it is easy to prove that the Gower distance kernel and the homoscedastic hypersphere one are equivalent: there is only one categorical hyperparameter and we can check in Tab. 2 that $\exp(-0.23015) = 0.7944$. On this particular test case, all the correlations are positive and so, our squared exponential homoscedastic hypersphere kernel and the original homoscedastic hypersphere kernel of Pelamatti *et al.* [8] are equivalent as they can be restricted to angle in $[0, \frac{\pi}{2}]$ as mentioned in Remark 3. A negative correlation would have been modeled by a correlation value close to 0 thanks to the exponential kernel.

4.2.2 A categorical cosine problem ($n = 1$, $m = 0$, $l = 1$ and $L_1 = 13$)

Let consider the cosine problem with two groups example proposed by Roustant *et al.* in [11] to show the behaviour of a matrix approach for categorical kernels. In this problem, the objective function f depends on a continuous variable in $[0, 1]$ and on a categorical variable with 13 levels. Appendix 6.3 provides a detailed description of this function. Let $w = (x, c)$ be a given point with x being the continuous variable and c being the categorical variable, $c \in \{1, \dots, 13\}$. There are two groups of curves corresponding to levels 1 to 9 and levels 10 to 13 with strong positive within-group correlations, and strong negative between-group correlations.

In this example, the number of relaxed dimensions for continuous relaxation is 14. A LHS DoE with 98 points (14×7 , if 7 points per dimension are considered) is chosen to build the Gaussian process models. The associated mean posterior models are shown on Fig. 2 for Gower distance (GD), continuous relaxation (CR), squared exponential homoscedastic hypersphere (EHH), and the full general (FE) kernels. The number of hyperparameters to optimize is therefore 2 for GD, 14 for CR, 79 for EHH and 92 for the FE kernel as indicated in Tab. 3. One can see, on Fig. 2, that the EHH model is the only one where every value remains properly within the interval $[-1, 1]$. It should also be the case when using the FE kernel but this kernel adds a lot of irrelevant parameters leading to an harder optimization problem. To quantify this assumption, we compute the root mean square error (RMSE) for every model as

$$\text{RMSE} = \sqrt{\sum_{i=1}^n \frac{1}{n} \left(\hat{f}(w_i) - f(w_i) \right)^2} \quad (22)$$

where n is the size of the validation set, $\hat{f}(w_i)$ is the prediction of our GP model at point w_i and $f(w_i)$ is the associated true value. The values are reported in Tab. 3. The validation set consists of 13000 evenly spaced points (see Appendix 6.3). As expected, the more the hyperparameters in the kernel, the better the induced GP model, as it can be seen from the decreasing RMSE

(from 30.079 to 2.941) in Tab. 3. For each kernel, the CPU time is provided: GD kernel takes 1.4 seconds to compute, CR kernel takes 24.5 seconds, and EHH takes 514.5 seconds to compute which motivates the use of a reduced order model. As mentioned earlier, the FE kernel with 92 hyperparameters on Fig. 2d shows poor performance in terms of CPU time (642 seconds) and RMSE (22.61) compared to the EHH kernel even though they are theoretically equivalent. Therefore, this FE kernel will not be considered for practical use cases.

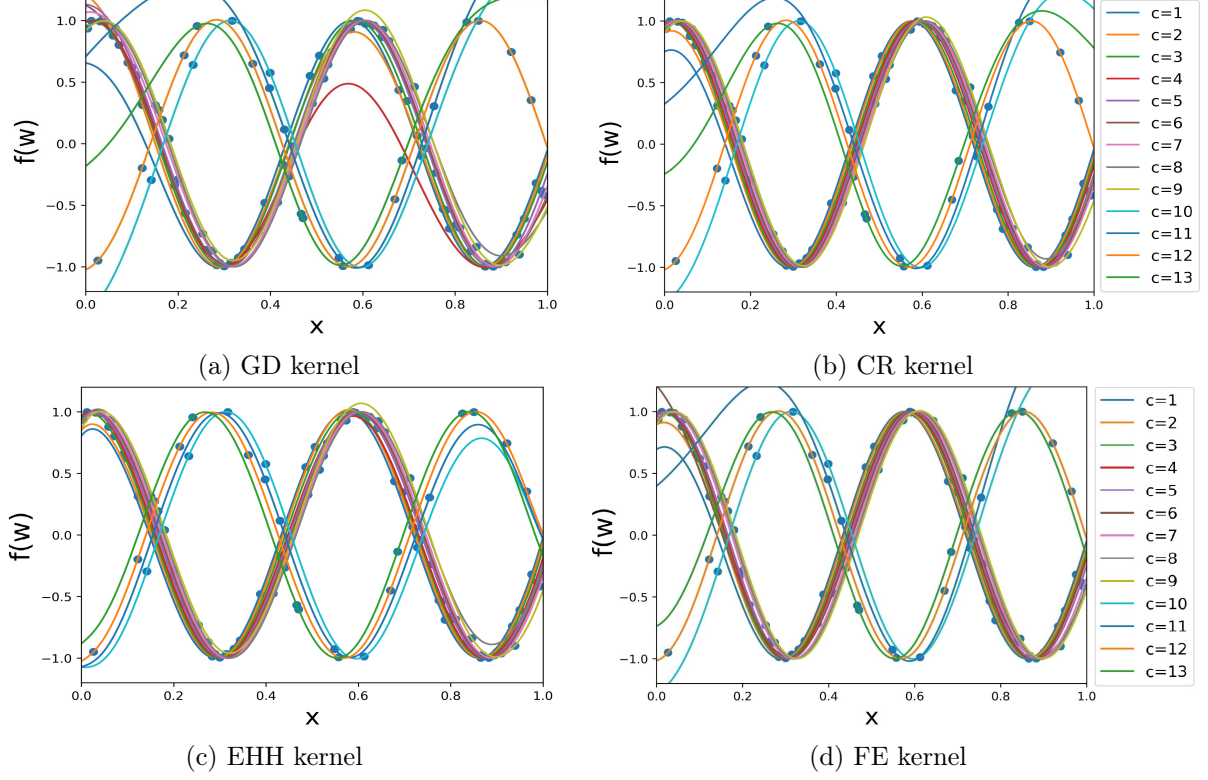


Figure 2: Mean predictions for our proposed model using different kernels over the matrix Θ_1 for the cosine problem with a 98 point DoE.

Table 3: Kernel comparison for the cosine test case

Kernel	# of Hyperparam.	RMSE	CPU time (s)
GD	2	30.079	1.4
CR	14	22.347	24.5
EHH	79	2.941	514.5
FE	92	22.610	642.0

The estimated correlation matrix $R_i = R_1^{cat}$ is shown in Fig. 3. For two given levels $\{\ell_r^1, \ell_s^1\}$, the correlation term $[R_1]_{\ell_r^1, \ell_s^1}$ is in blue for correlation value close to 1, in white for correlations close to 0 and in red for value close to -1; moreover the thicker the ellipse, the higher the correlation and we can see that the correlation between a level and itself is always 1. As expected, with GD kernel, there is only one estimated "mean correlation" as in Fig. 3a. For CR kernel (see Fig. 3b), the most important levels (1 to 9) are strongly correlated (in blue) with one another and the

other levels (10 to 13) that should also have been correlated are badly estimated because of the kernel limitations that neglected them. In contrast, the EHH kernel (see Fig. 3c) gives a good approximation of the real correlations as it recovers the two groups of highly correlated levels. We recover the levels 1 to 9 as strongly similar and the levels 10 to 13 as strongly similar which is a good point but the 2 groups, even if less similar, are still positively correlated with one another. The latter between-group correlations should have been negative but the squared exponential kernel does not allow negative values.

As previously mentioned, the FE kernel (see Fig. 3d) that combines both CR and EHH hyperparameters adds irrelevant complexity while being equivalent to the EHH kernel. For this reason, it should not be considered for real applications.

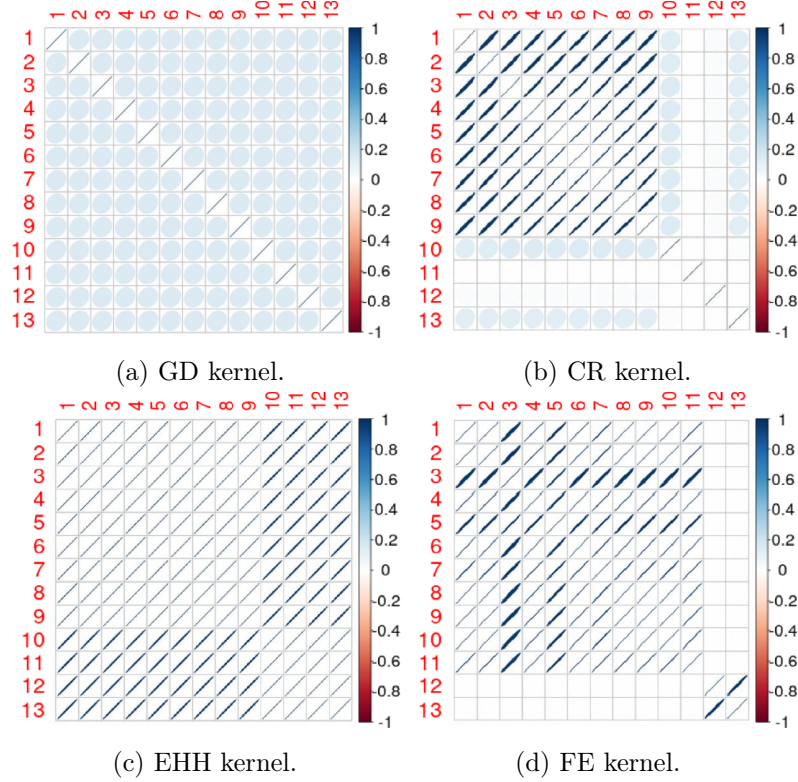


Figure 3: Correlation matrix R_1^{cat} using different choices for Θ_1 on the cosine problem with a DoE of 98 points.

We compare in Fig. 4 our EHH kernel (see Fig. 4a) with the homoscedastic hypersphere model of Pelamatti *et al.* [8] that allows negative values (see Fig. 4b with some red correlations). By choosing the correlation matrix of Fig. 4b for homoscedastic hypersphere, we obtain a likelihood of around 210 against 138 for our EHH kernel with only positive values. Nevertheless, even if the homoscedastic hypersphere model is more general than our model, the two RMSE are of the same order of magnitude (around 3 for EHH and 5 for homoscedastic hypersphere), which indicates similar performances.

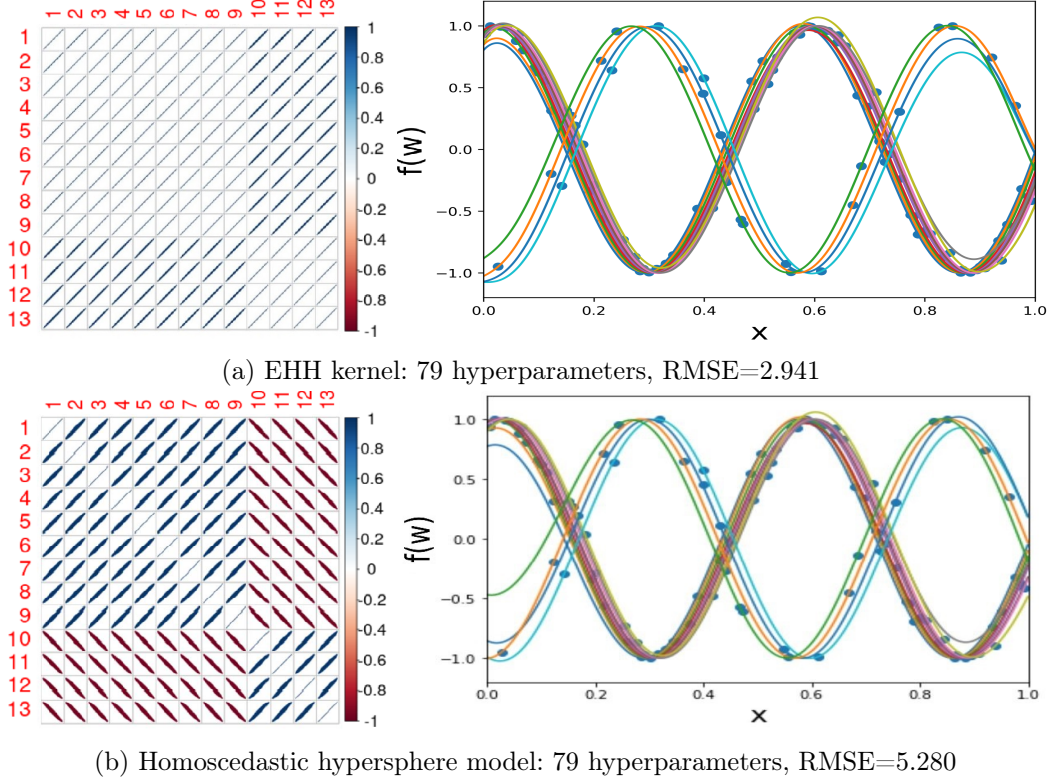


Figure 4: Comparison results between our model and Homoscedastic hypersphere [8] on the cosine problem using a DoE of 98 points.

On this particular test case, with a 98 point DoE, the more general the kernel, the better the performance and precision of the resulting GP. On Fig. 5, we draw 6 LHS DoEs of different sizes and we plot the RMSE and computational time for the kernels to see how they behave for different DoE sizes.

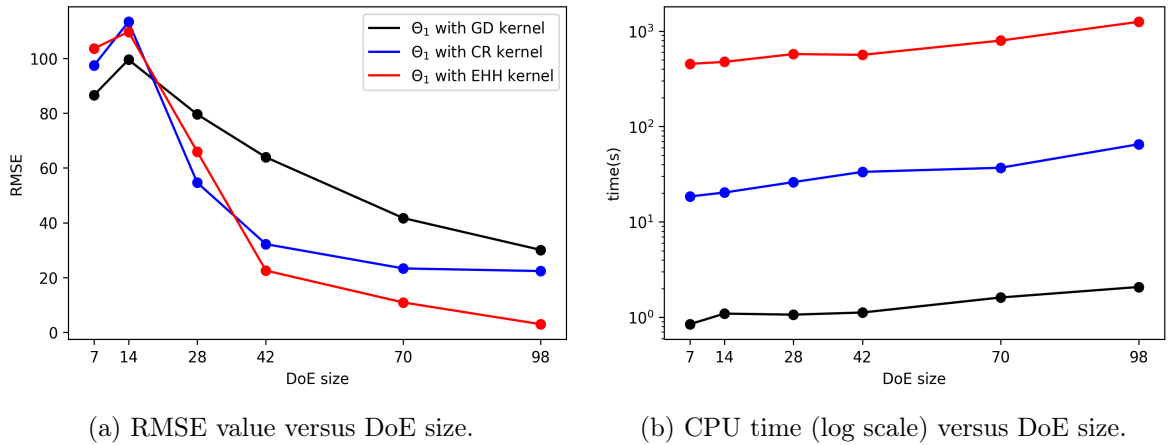


Figure 5: RMSE and CPU time to compute models with respect to DoE size.

As expected, when the size of the DoE is too small for the problem (here smaller than 15 points), the three model behaviours are similarly bad because too little information is available for the hyperparameters optimization. However, when the size of the DoE is sufficiently large, we found the same hierarchy we found with 98 points on Fig. 2 and the more complex the model, the faster the RMSE convergence. Nevertheless, on Fig. 5b, we can see that the computational costs of the models scale hardly with the DoE size on a logarithmic scale.

4.3 Application to engineering problems

To validate and compare our method on real applications, we will consider two engineering problems of different scale to analyze the model behaviour. In Section 4.3.1, we will present an engineering beam bending problem and in Section 4.3.2, we will present a complex system problem from aircraft design.

4.3.1 Cantilever beam bending problem ($n = 2$, $m = 0$, $l = 1$ and $L_1 = 12$)

A first engineering problem commonly use for model validation is the beam bending problem in its linear elasticity range [11, 49]. This problem is illustrated on Fig. 6a and consists of a cantilever beam loaded at its free extremity with a force F . As in Cheng *et al.* [49], we choose a constant Young modulus of $E = 200\text{GPa}$ and a load of $F = 50\text{kN}$. Moreover, as in Roustant *et al.* [11], we consider 12 possible cross-sections: there are 4 possible shapes, illustrated in Fig. 6b that could be hollow, thick or full. For a given cross-section (shape and thickness), its size is determined by its surface S . Every cross section is associated with a normalized moment of inertia \tilde{I} about the neutral axis. The latter is a latent variable associated to the beam shape [50].

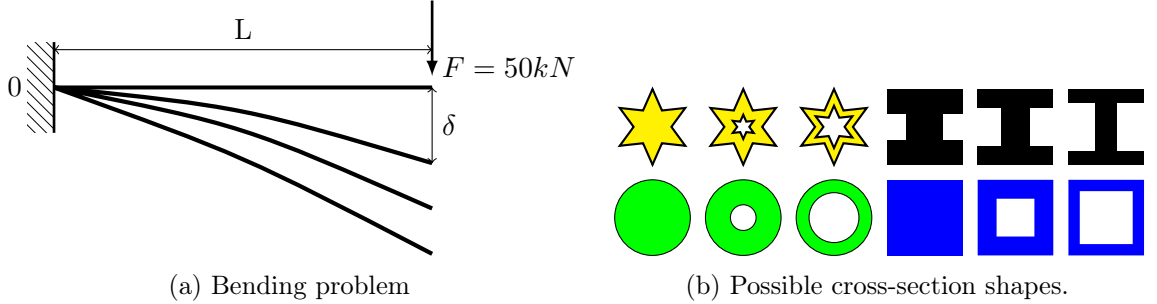


Figure 6: Cantilever beam problem.

Therefore, the problem to model has two continuous variables: the length $L \in [10, 20]$ (in m) and the surface $S \in [1, 2]$ (in m^2) and one categorical variable \tilde{I} with 12 levels. The tip deflection, at the free end, δ is given by

$$\delta = f(\tilde{I}, L, S) = \frac{F}{3E} \frac{L^3}{S^2 \tilde{I}}$$

To compare our models, we draw a 98 point LHS as training set and the validation set is a grid of $12 \times 30 \times 30 = 10800$ points. For both squared exponential and absolute exponential kernels, the RMSE, likelihood and computational time for every model are shown in Tab. 4. We recall that squared exponential and absolute exponential kernels differ only on the continuous variables and are the same for the categorical part. As expected, the computational time and the likelihood increase when the model is more complex. The DoE seems of sufficient size for this

problem as the computed RMSE of Eq. (22) (*i.e.*, the total displacement error) decreases with the model complexity.

Table 4: Results of the cantilever beam models

Categorical kernel	Continuous kernel	Displacement error (cm)	Likelihood	Time (s)
GD	squared exponential	1.3858	111.13	8.02
CR	squared exponential	1.1604	162.26	89.1
EHH	squared exponential	0.1247	256.90	2769.4
GD	absolute exponential	3.2403	74.48	14.71
CR	absolute exponential	3.0918	99.00	260.1
EHH	absolute exponential	2.0951	102.48	19784

In Fig. 7, we have drawn the correlation matrix found between the cross-section shape (the resulting R_1 correlation matrix) for the three models. On the figure below, the higher the correlation, the thicker the ellipse.

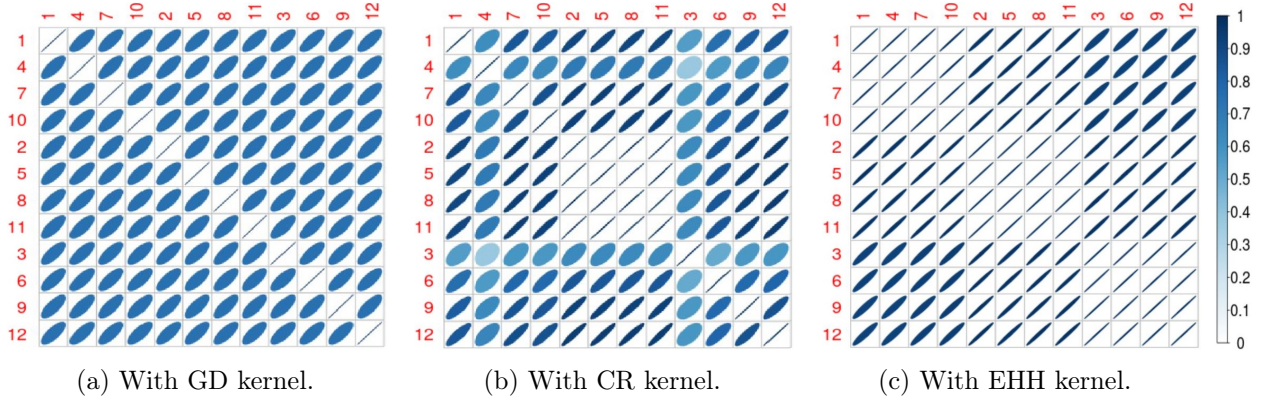


Figure 7: Correlation matrix R_1^{cat} using different choices for Θ_1 for the categorical variable \tilde{I} from the cantilever beam problem.

As expected, we have 3 groups of 4 shapes depending on their respective thickness (respectively, the levels $\{1,4,7,10\}$ the levels $\{2,5,8,11\}$ and the levels $\{3,6,9,12\}$). The more the thickness is similar, the higher the correlation: the thickness has more impact than the shape of the cross-section on the tip deflection. However, given the database, two points with similar L and S values will have similar output whatever the cross-section. The effect of the cross-section on the output is always the same (in the form of $\frac{1}{l}$) leading to an high correlation after maximizing the likelihood. In Fig. 7c, with the EHH kernel, we can distinguish the 3 groups of 4 shapes and, because the correlations are close to 1, the homoscedastic hyperphere model [8] would lead to the same correlation matrix. Also, with the CR kernel of Fig. 7b, the medium thick group $\{2,5,8,11\}$ being correlated with both the full and the hollow group, its correlation values are the higher whereas the correlation hyperparameters associated to the two other groups are smaller. For the GD model in Fig. 7a, there is only one mean positive correlation value as before.

4.3.2 Aircraft design application ($n = 10$, $m = 0$, $l = 2$ and $L_1 = 9$, $L_2 = 2$)

The “**DRAGON**” aircraft concept has been introduced by ONERA in 2019 [51] within the scope of the European CleanSky 2 program ³ which sets the objective of 30% reduction of CO2 emissions by 2035 with respect to 2014 state of the art. The employment of a distributed propulsion comes at a certain cost; a turboelectric propulsive chain is necessary to power the electric fans which brings additional complexity and weight. The turboelectric propulsive chain being an important weight penalty, it is of particular interest to optimize the chain and particularly the number and type of each component, characterized by some discrete values. The definition of the architecture variable is given in Tab. 5a and the definition of the turboshaft layout is given in Tab. 5b. For the sake of simplicity, we restrict the optimization problem to the case of two electric cores and generators but more optimizations have been performed in [1].

Architecture number	Number of motors	Number of cores	Number of generators
1	8	2	2
2	12	2	2
3	16	2	2
4	20	2	2
5	24	2	2
6	28	2	2
7	32	2	2
8	36	2	2
9	40	2	2

(a) Definition of the architecture variable and its 9 associated levels.

Layout	Position	y ratio	Tail	VT aspect ratio	VT taper ratio
1	under wing	0.25	without T-tail	1.8	0.3
2	behind	0.34	with T-tail	1.2	0.85

(b) Definition of the turboshaft layout variable and its 2 associated levels.

Table 5: Categorical variable definition

The analysis of “**DRAGON**” is treated with Overall Aircraft Design method in FAST-OAD [52]. We are considering the following problem described in Tab. 6.

³<https://www.cleansky.eu/technology-evaluator>

Table 6: Definition of the “DRAGON” optimization problem.

	Function/variable	Nature	Quantity	Range
Model	Fuel mass	cont	1	
with respect to	Fan operating pressure ratio	cont	1	[1.05, 1.3]
	Wing aspect ratio	cont	1	[8, 12]
	Angle for swept wing	cont	1	[15, 40] ($^{\circ}$)
	Wing taper ratio	cont	1	[0.2, 0.5]
	HT aspect ratio	cont	1	[3, 6]
	Angle for swept HT	cont	1	[20, 40] ($^{\circ}$)
	HT taper ratio	cont	1	[0.3, 0.5]
	TOFL for sizing	cont	1	[1800., 2500.] (m)
	Top of climb vertical speed for sizing	cont	1	[300., 800.] (ft/min)
	Start of climb slope angle	cont	1	[0.075., 0.15.] (rad)
	Total continuous variables		10	
	Architecture	cat	9 levels	{1,2,3, ..., 7,8,9}
	Turboshaft layout	cat	2 levels	{1,2}
	Total categorical variables		2	
	Total relaxed variables		21	

Twice, we draw 250 points by LHS. Over the first DoE, that is the training set, we build the model to predict the fuel mass and over the second one, we validate our prediction and compute the RMSE reported in Tab. 7. In this case, the number of hyperparameters is 12 for GD kernel, 21 for CR kernel and 47 for EHH kernel. Evaluating the function is costly, around 4 minutes for a single point. We observed similar performances for all models, the performance is mostly determined by the choice of the continuous kernel. For a problem that has that many variables, it seems useless and impractical to use a complicated model, the GD kernel being already performing well. On Fig. 8, we plot, for the three kernels, the approximate correlation matrices for the first categorical variable. As we can see, when considering the general EHH kernel, as in Fig. 8c, the closer the levels, the higher the correlation. In fact, in this case, the only difference between two levels is the number of motors. Therefore, the more similar the number of motors, the more similar the fuel consumption. Given that, we expect, when considering CR kernel as in Fig. 8b that the higher correlation should appear "in the middle" {4,5,6} as these levels are meant to be the most correlated with the others. This is what happens to a certain extent but the levels 7 and 8 are weirdly appearing too much correlated with one another. This could be a numerical problem, the optimization being hard with that many variables and hyperparameters. As before, the GD kernel is the less precise and just give a mean correlation over the whole space as in Fig. 8a. In Fig. 9, we plot, for the three methods, the approximated correlation matrices for the second categorical variable. There is only two engine layouts so there is only one correlation. In this case, the correlation is positive indicating that the plane behave in the same way no matter the layout.

Table 7: Results of the aircraft models based on a 250 point validation set

kernel	number of hyperparameters	kernel	fuel error (kg)	time (s)
GD	12	squared exponential	2115	65
CR	21	squared exponential	2068	210
EHH	47	squared exponential	2147	9450
GD	12	absolute exponential	1666	65
CR	21	absolute exponential	1664	210
EHH	47	absolute exponential	1593	9295

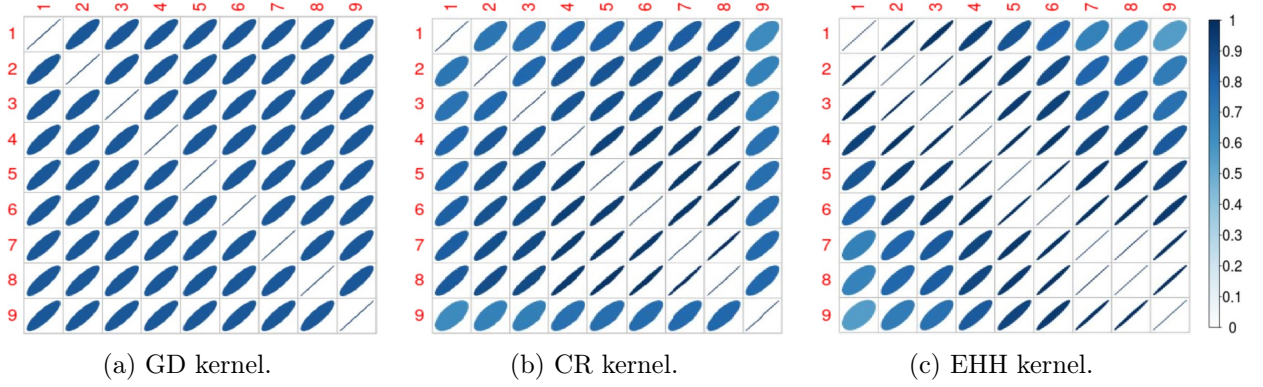


Figure 8: Correlation matrix R_1^{cat} using different choices for Θ_1 for the turboelectric architecture variable.

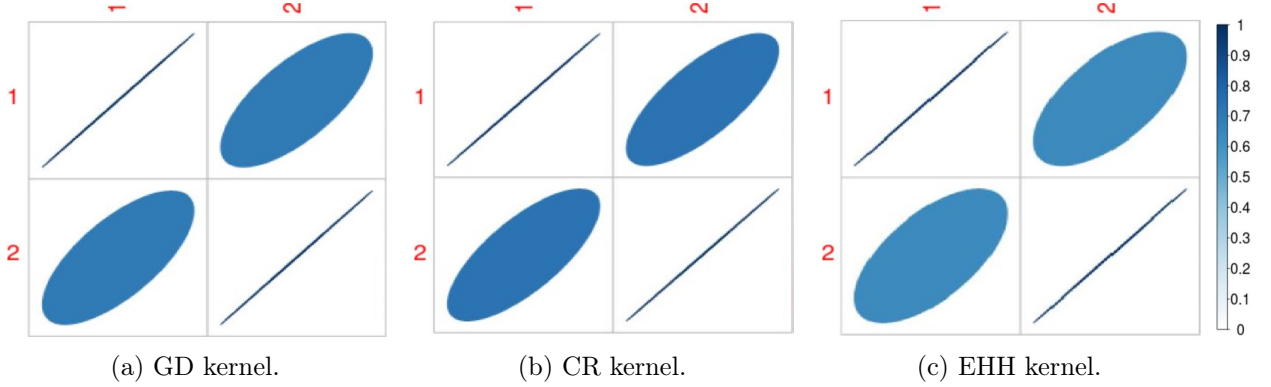


Figure 9: Correlation matrix R_2^{cat} using different choices for Θ_2 for the turboshaft layout variable.

One can note that increasing the number of motors or changing a layout will not change the way an aircraft flies. For example, having more motors will only increase the fuel consumption by a given factor. The latter will always remain positive and related to the continuous variables. Hence, in this test case, we do not have opposite effects between two categorical levels.

In most industrial applications, radically opposite effects over a complex system do not occur so often. For instance, on the industrial applications that can be found on the literature, there was not a clear need for negative correlation values [8, 11, 14]. Therefore, in practice, the exponential model is not that limiting compared to the homoscedastic hypersphere model.

5 Conclusion

In this work, we have proposed a class of kernels for GP models that extends the exponential continuous kernels to the mixed-categorical setting. We showed that this class of kernels generalizes Gower distance and continuous relaxation based kernels. A classification between the proposed kernels as well as a proof of the SPD nature of the resulting correlation matrices have been also proposed. Numerical illustrations on analytical toy problems showed the good potential of the

proposed kernels to reduce the number of hyper-parameters and thus the computational time. The implementation of our proposed method has been released in the toolbox SMT v1.4⁴.

When considering complex kernels, a good approach would be to use a model reduction technique such as Kriging with Partial Least Squares (KPLS) [53] that is derived from the construction of the correlation matrix via a kernel function. KPLS is an adaptation of the Partial Least Squares regression for exponential kernels and is used to reduce the number of hyperparameters and handle a large number of mixed inputs. Further works will consider to include such dimension reduction techniques to improve the computational efficiency of our model and tackle higher dimensional problems.

Acknowledgements

This work is part of the activities of ONERA - ISAE - ENAC joint research group. The research presented in this paper has been performed in the framework of the AGILE 4.0 project (Towards Cyber-physical Collaborative Aircraft Development) and has received funding from the European Union Horizon 2020 Programme under grant agreement n° 815122. We thank Raul Carreira Rufato (ISAE-Supaero MSc) for his contribution to Gower distance implementation, and Dr. Eric Nguyen Van (ONERA) and Christophe David (ONERA) for their contribution to DRAGON aircraft design. The authors are grateful to the partners of the AGILE 4.0 consortium for their contribution and feedback.

6 Appendix

To begin with, in Appendix 6.1, we give the parameterization that allows us to obtain the continuous relaxation model from our more general one. Then, this appendix describes the two analytical test cases more in details. In Appendix 6.2, a description of the blue/red case is given and in Appendix 6.3, the cosine test case is detailed.

6.1 Continuous relaxation is a particular instance of our proposed FE Kernel.

To show that CR is a particular instance of FE, it suffices to show that the matrix $\Phi(\Theta_i)$ is diagonal whenever Θ_i is set to a diagonal one. In fact, assume that we have, in our general model, $[\Theta_i]_{j \neq j'} = 0$, $\forall (j, j') \in \{1, \dots, L_i\}$. Knowing that $\cos(0) = 1$ and $\sin(0) = 0$, the matrix $C(\Theta_i)$ writes as

$$C(\Theta_i) = \begin{bmatrix} 1 & 0 & 0 & 0 \\ 1 & 0 & \dots & 0 \\ \vdots & \vdots & \ddots & 0 \\ 1 & 0 & 0 & 0 \end{bmatrix} \quad \text{and} \quad C(\Theta_i)C(\Theta_i)^\top = \begin{bmatrix} 1 & 1 & 1 & 1 \\ 1 & 1 & \dots & 1 \\ \vdots & \vdots & \ddots & 1 \\ 1 & 1 & 1 & 1 \end{bmatrix}$$

Therefore, we also have

$$[\Phi(\Theta_i)]_{j \neq j'} = \frac{\log \epsilon}{2} ([C(\Theta_i)C(\Theta_i)^\top]_{j, j'} - 1) = 0 \quad \forall (j, j') \in \{1, \dots, L_i\}$$

⁴<https://smt.readthedocs.io/en/latest/>

that is the continuous relaxation kernel. □

6.2 2D blue/red test case

This test case has one categorical variable with two levels: 'blue' or 'red' and one continuous variable in $[0, 4]$.

- The blue DoE of 3 points is the following: $x = \{0, 1, 4\}$, $y = \{0, 9, 16\}$
- The red DoE of 4 points is the following: $x = \{0, 1, 2, 3\}$, $y = \{0, 1, 8, 27\}$

Therefore, we have a DoE consisting of 7 points either blue or red, with continuous value ranging between 0 and 4 and taking value between 0 and 27.

6.3 Categorical cosine case

This test case has one categorical variable with 13 levels and one continuous variable in $[0, 1]$ [11]. Let $w = (x, c)$ be a given point with x being the continuous variable and c being the categorical variable, $c \in \{1, \dots, 13\}$.

$$f(w) = \cos\left(\frac{7\pi}{2}x + \left(0.4\pi + \frac{\pi}{15}c\right) - \frac{c}{20}\right), \quad \text{if } c \in \{1, \dots, 9\}$$

$$f(w) = \cos\left(\frac{7\pi}{2}x - \frac{c}{20}\right), \quad \text{if } c \in \{10, \dots, 13\}$$

The reference landscapes of the objective function (with respect to the categorical choices) are drawn on Fig. 10.

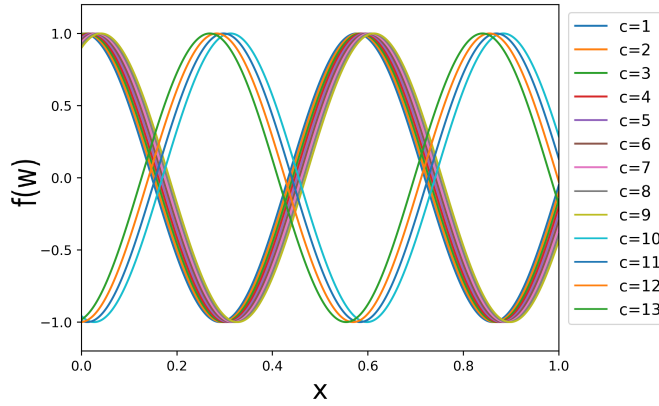


Figure 10: Landscape of the cosine test case from [11].

The DoE is given by a LHS of 98 points. Our validation set is a evenly spaced grid of 1000 points in x ranging for every of the 13 categorical levels for a total of 13000 points.

References

- [1] P. Saves, E. Nguyen Van, N. Bartoli, Y. Diouane, T. Lefebvre, C. David, S. Defoort, J. Morlier, Bayesian optimization for mixed variables using an adaptive dimension reduction process: applications to aircraft design, in: AIAA SciTech 2022, 2022.
- [2] J. Snoek, O. Rippel, K. Swersky, R. Kiros, N. Satish, N. Sundaram, M. Patwary, M. Prabhat, R. Adams, Scalable bayesian optimization using deep neural networks, in: International conference on machine learning, 2015.
- [3] A. F. López-Lopera, D. Idier, J. Rohmer, F. Bachoc, Multioutput gaussian processes with functional data: A study on coastal flood hazard assessment, Reliability Engineering & System Safety 218 (2022) 108139.
- [4] P. Ghasemi, M. Karbasi, A. Zamani Nouri, M. Sarai Tabrizi, H. M. Azamathulla, Application of gaussian process regression to forecast multi-step ahead spei drought index, Alexandria Engineering Journal 60 (2021) 5375–5392.
- [5] Y. Diouane, S. Gratton, X. Vasseur, L. N. Vicente, H. Calandra, A parallel evolution strategy for an earth imaging problem in geophysics, Optim. Eng. 17 (2016) 3–26.
- [6] C. K. Williams, C. E. Rasmussen, Gaussian processes for machine learning, MIT press Cambridge, MA, 2006.
- [7] D. G. Krige, A statistical approach to some basic mine valuation problems on the witwatersrand, Journal of the Southern African Institute of Mining and Metallurgy 52 (1951) 119–139.
- [8] J. Pelamatti, L. Brevault, M. Balesdent, E.-G. Talbi, Y. Guerin, Efficient global optimization of constrained mixed variable problems, Journal of Global Optimization 73 (2019) 583–613.
- [9] Q. Zhou, P. Z. G. Qian, S. Zhou, A simple approach to emulation for computer models with qualitative and quantitative factors, Technometrics 53 (2011) 266–273.
- [10] X. Deng, C. D. Lin, K. Liu, R. K. Rowe, Additive gaussian process for computer models with qualitative and quantitative factors, Technometrics 59 (2017) 283–292.
- [11] O. Roustant, E. Padonou, Y. Deville, A. Clément, G. Perrin, J. Giorla, H. Wynn, Group kernels for gaussian process metamodels with categorical inputs, SIAM Journal on Uncertainty Quantification 8 (2020) 775–806.
- [12] E. C. Garrido-Merchán, D. Hernández-Lobato, Dealing with categorical and integer-valued variables in bayesian optimization with gaussian processes, Neurocomputing 380 (2020) 20–35.
- [13] M. Halstrup, Black-Box Optimization of Mixed Discrete-Continuous Optimization Problems, Ph.D. thesis, TU Dortmund, 2016.
- [14] J. Cuesta-Ramirez, R. Le Riche, O. Roustant, G. Perrin, C. Durantin, A. Gliere, A comparison of mixed-variables bayesian optimization approaches, Advanced Modeling and Simulation in Engineering Sciences 9 (2021) 1–29.
- [15] F. Hutter, H. Hoos, K. Leyton-Brown, Sequential model-based optimization for general algorithm configuration, in: International Conference on Learning and Intelligent Optimization, 2011.
- [16] J. S. Bergstra, R. Bardenet, Y. Bengio, B. Kégl, Algorithms for hyper-parameter optimization, in: 25th Annual Conference on Neural Information Processing Systems, 2011.

- [17] L. Bliet, A. Guijt, S. Verwer, M. de Weerd, Black-box mixed-variable optimisation using a surrogate model that satisfies integer constraints, in: *Proceedings of the Genetic and Evolutionary Computation Conference Companion*, 2021.
- [18] T. Papalexopoulos, C. Tjandraatmadja, R. Anderson, J. P. Vielma, D. Belanger, Constrained discrete black-box optimization using mixed-integer programming, 2021.
- [19] Z. Nie, J. Racine, The crs package: nonparametric regression splines for continuous and categorical predictors, *R Journal* 4 (2012) 48–56.
- [20] M. Herrera, A. Guglielmetti, M. Xiao, R. F. Coelho, Metamodel-assisted optimization based on multiple kernel regression for mixed variables, *Structural and multidisciplinary optimization* 49 (2014) 979–991.
- [21] A. Moraglio, , A. Kattan, Geometric generalisation of surrogate model based optimisation to combinatorial spaces, in: *Evolutionary Computation in Combinatorial Optimization*, 2011.
- [22] M. M. Zuniga, D. Sinoquet, Global optimization for mixed categorical-continuous variables based on gaussian process models with a randomized categorical space exploration step, *INFOR: Information Systems and Operational Research* 58 (2020) 310–341.
- [23] D. Nguyen, S. Gupta, S. Rana, A. Shilto, S. Venkatesh, Bayesian optimization for categorical and category-specific continuous inputs, in: *AAAI-20 Technical Tracks*, 2020.
- [24] S. Roy, W. A. Crossley, B. K. Stanford, K. T. Moore, J. S. Gray, A mixed integer efficient global optimization algorithm with multiple infill strategy - applied to a wing topology optimization problem, in: *AIAA Scitech 2019 Forum*, 2019.
- [25] M. A. Abramson, C. Audet, J. Dennis, Filter pattern search algorithms for mixed variable constrained optimization problems, *Pacific Journal of Optimization* 3 (2007) 477–500.
- [26] M. A. Bouhlel, J. T. Hwang, N. Bartoli, R. Lafage, J. Morlier, J. R. A. Martins, A python surrogate modeling framework with derivatives, *Advances in Engineering Software* 135 (2019) 102662.
- [27] M. Krügener, J. Zapata Usandivaras, , M. Bauerheim, A. Urbano, Coaxial-injector surrogate modeling based on reynolds-averaged navier–stokes simulations using deep learning, *Journal of Propulsion and Power* 38 (2022) 783–798.
- [28] J. Li, M. Zhang, C. M. J. Tay, N. Liu, Y. Cui, S. C. Chew, B. C. Khoo, Low-reynolds-number airfoil design optimization using deep-learning-based tailored airfoil modes, *Aerospace Science and Technology* 121 (2022) 107309.
- [29] J. Li, M. Zhang, J. R. R. A. Martins, C. Shu, Efficient aerodynamic shape optimization with deep-learning-based geometric filtering, *AIAA Journal* 58 (2020) 4243–4259.
- [30] J. Zapata Usandivaras, M. Bauerheim, C. Benedicte, A. Urbano, Large eddy simulations and deep learning for the investigation of recess variation of a shear-coaxial injector, in: *Space Propulsion Conference 2022*, 2022.
- [31] D. Ming, D. Williamson, S. Guillas, Deep gaussian process emulation using stochastic imputation, *Technometrics* 0 (2022) 1–12.
- [32] M. F. Izzaturrahman, P. S. Palar, L. Zuhail, K. Shimoyama, Modeling non-stationarity with deep gaussian processes: Applications in aerospace engineering, in: *AIAA SciTech 2022 Forum*, 2021.
- [33] A. Forrester, A. Sobester, A. Keane, *Engineering Design via Surrogate Modelling: A Practical Guide*, Wiley, 2008.

- [34] D. Duvenaud, Automatic model construction with Gaussian processes, Ph.D. thesis, University of Cambridge, 2014.
- [35] R. J. Rossi, Mathematical statistics: an introduction to likelihood based inference, John Wiley & Sons, 2018.
- [36] H. Lee, Gaussian Processes, Springer Berlin Heidelberg, 2011, pp. 575–577.
- [37] D. Golovin, B. Solnik, S. Moitra, G. Kochanski, J. Karro, D. Sculley, Google vizier: A service for black-box optimization, in: Proceedings of the 23rd ACM SIGKDD International Conference on Knowledge Discovery and Data Mining, 2017.
- [38] R. C. Rufato, Y. Diouane, J. Henry, R. Ahlfeld, J. Morlier, A mixed-categorical data-driven approach for prediction and optimization of hybrid discontinuous composites performance, in: AIAA AVIATION 2022 Forum, 2022.
- [39] R. Rebonato, P. Jaekel, The most general methodology to create a valid correlation matrix for risk management and option pricing purposes, *Journal of Risk* 2 (2001) 17–27.
- [40] F. Rapisarda, D. Brigo, F. Mercurio, Parameterizing correlations: a geometric interpretation, *IMA Journal of Management Mathematics* 18 (2007) 55–73.
- [41] P. Z. G. Qian, H. Wu, C. F. J. Wu, Gaussian process models for computer experiments with qualitative and quantitative factors, *Technometrics* 50 (2008) 383–396.
- [42] J. Hadamard, Sur quelques applications de l’indice de Kronecker, Bussiere, 1910.
- [43] R. B. Bapat, T. E. S. Raghavan, Nonnegative Matrices and Applications, Cambridge University Press, 1997.
- [44] I. J. Schoenberg, Metric spaces and positive definite functions, *Transactions of the American Mathematical Society* 44 (1938) 522–536.
- [45] R. A. Horn, C. R. Johnson, Matrix analysis, Cambridge university press, 2012.
- [46] N. Y. Vilenkin, A. U. Klimyk, Representations of Lie groups and special functions, Springer, 1995.
- [47] M. J. D. Powell, A direct search optimization method that models the objective and constraint functions by linear interpolation, Springer, 1994, pp. 51–67.
- [48] R. Jin, W. Chen, A. Sudjianto, An efficient algorithm for constructing optimal design of computer experiments, *Journal of Statistical Planning and Inference* 2 (2005) 545–554.
- [49] G. H. Cheng, A. Younis, K. H. Hajikolaie, G. G. Wang, Trust region based mode pursuing sampling method for global optimization of high dimensional design problems, *Journal of Mechanical Design* 137 (2015) 021407.
- [50] N. Oune, R. Bostanabad, Latent map gaussian processes for mixed variable metamodeling, *Computer Methods in Applied Mechanics and Engineering* 387 (2021) 114128.
- [51] P. Schmollgruber, C. Döll, J. Hermetz, R. Liaboeuf, M. Ridel, I. Cafarelli, O. Atinault, C. François, B. Paluch, Multidisciplinary exploration of DRAGON: an ONERA hybrid electric distributed propulsion concept, in: AIAA Scitech 2019, 2019.
- [52] C. David, S. Delbecq, S. Defoort, P. Schmollgruber, E. Benard, V. Pommier-Budinger, From FAST to FAST-OAD: An open source framework for rapid overall aircraft design, *IOP Conference Series: Materials Science and Engineering* 1024 (2021) 012062.

- [53] M. A. Bouhlef, N. Bartoli, R. Regis, A. Otsmane, J. Morlier, Efficient global optimization for high-dimensional constrained problems by using the kriging models combined with the partial least squares method, *Engineering Optimization* 50 (2018) 2038–2053.